



# Effect of Submarine Slope Inclination on Seismic Response of Deep Tunnels

Wang Xiong<sup>1,2</sup>, Zhendong Shan<sup>\*1,2</sup>

<sup>1</sup>Key Laboratory of Earthquake Engineering and Engineering Vibration, Institute of Engineering Mechanics, China Earthquake Administration, Harbin 150080, P.R. China

<sup>2</sup>Key Laboratory of Earthquake Disaster Mitigation, Ministry of Emergency Management, Harbin 150080, P.R. China

\*Corresponding author: shanzhendong@gmail.com

**Abstract.** Unlike horizontal seabeds, offshore seabeds typically exhibit varying inclination angles. This inclined topography alters both the propagation paths and reflection characteristics of seismic waves, leading to significant variations in seismic impacts across different seabed zones. As a key structural element on offshore seabeds, analyzing extreme internal forces in tunnel cross-sections enables more economical and safer designs for different tunnel segments. Based on a layered seabed model (seawater-sediment-bedrock), this study calculates the stress field at the tunnel center under P-waves transmitted from bedrock, and further determines peak internal forces in tunnel linings. By systematically investigating the effects of seabed inclination angle, sediment permeability coefficient on lining force extremes, this research provides critical insights for offshore tunnel design. Key findings include: Seabed inclination predominantly influences seismic response characteristics under long-period ground motions, with tunnel lining thrust and bending moments escalating significantly as inclination increases; Except in low-frequency ranges, the most pronounced inclination effects on lining forces occur near the seabed's natural frequency; At constant inclination, reduced permeability coefficients lead to progressive increases in lining internal forces under low-frequency seismic actions.

**Keywords:** Tunnel, Lining internal forces, Seawater-sediment-bedrock model, Double-layer site, Permeability coefficient

## 1 Introduction

In recent years, China has explicitly included the construction of undersea tunnels in its national major infrastructure planning. At the same time, it has emphasized the need to strengthen urban underground space development and promote the construction of comprehensive transportation systems. The completion of the Shantou Bay Undersea Tunnel on March 26 is recognized as an important component of the national coastal corridor. The completion of this tunnel further consolidates China's leading position in infrastructure construction, while also shortening transportation times and promoting

regional economic integration. As a typical marine engineering structure, undersea tunnels are often located on sloping seabeds. Compared to surface-level tunnels, undersea stratum tunnels have the advantages of higher concealment and lower risks of collision or damage, making them the preferred choice for major projects. The locations of China's undersea tunnel constructions often overlap significantly with the distribution of seismic zones in the country. For example, the area where the completed Shantou Bay Undersea Tunnel is located is classified as a seismic fortification area of VII degree or higher, belonging to a moderate-strong earthquake activity zone. Historically, this region has experienced multiple earthquakes of magnitude 6 or above, posing potential risks of strong earthquakes. Marine seismic activities can severely damage the stability of seabed structures, thereby affecting the stability of nearby seabed structures. To ensure the safety of undersea stratum tunnels, it is necessary to study the seismic dynamic response of tunnels within the seawater-sloping seabed-basement rock system.

Over the past two decades, extensive research has been conducted on the dynamic cross-sectional responses of tunnels under seismic loads. Hany EI Naggar et al.<sup>[1]</sup> modeled tunnel linings as thin-walled shells within linear elastic soil/rock or thick-walled cylinders, deriving solutions for lining forces with both slip and non-slip conditions at lining-ground interfaces. Kontoe et al.<sup>[2]</sup> employed an equivalent linear approach to approximate nonlinear behavior. Huang et al.<sup>[3]</sup> developed simplified analytical solutions for stress and deformation in circular composite linings with arbitrary layers under in-plane shear waves. Duan et al.<sup>[4]</sup> established analytical expressions for thrust and bending moments in semi-space circular tunnels under obliquely incident P-waves. Gong et al.<sup>[5]</sup> proposed unified analytical solutions for seismic-induced stresses and displacements in deeply buried tunnels within saturated orthotropic rock formations. Zhao et al.<sup>[6]</sup> derived analytical solutions for thrust and bending moments in multi-layered circular tunnels subjected to oblique P- and SV-waves. Yu et al.<sup>[7]</sup> investigated stresses and displacements in deeply buried tunnels with isolation layers under SH-wave excitation, while Duan et al.<sup>[8]</sup> introduced novel analytical solutions for tunnel behavior under combined static and seismic loads. These methodologies primarily address inland tunnel analysis. For subsea applications, Zhao et al.<sup>[9]</sup> developed analytical solutions for composite-lined tunnels under Rayleigh wave excitation. Zhao et al.<sup>[10]</sup> extended their work to multi-layered seabed tunnels under both vertical and oblique P-/SV-waves. All assuming horizontal seabed conditions.

Growing attention has focused on inclined seabed responses to seismic and wave loads, given most offshore structures rest on sloping terrains. Feng and Price<sup>[11]</sup> examined hydrodynamic responses of floating/fixed structures under wave actions. Dou et al.<sup>[12]</sup> analyzed clayey sloping seabed behavior under wave loading, proposing improved formulas for critical failure assessment based on experimental data. Xu et al.<sup>[13]</sup> quantified seabed slope effects on pipeline responses, while Seyfipour and Walker<sup>[14]</sup> investigated pipeline downslope "walking" phenomena on partially inclined seabeds, recommending serpentine pipeline layouts as mitigation. Rafiei et al.<sup>[15]</sup> employed coupled FEM to evaluate wave-induced seabed instability, and Zhao and Jeng<sup>[16]</sup> developed an integrated mathematical model for wave-seabed interactions near breakwaters. Ni

and Teng<sup>[17]</sup> derived modified mild-slope equations for wave loading on porous seabeds. While these studies predominantly address wave-load responses, seismic behavior of structures on inclined seabeds remains underexplored.

The inclined seabed alters seismic wave propagation paths and reflection characteristics, leading to significant variations in ground motion across different zones. Frequency-dependent responses on sloping terrains further modify the distribution of low/high-frequency components compared to horizontal sites. This necessitates focused investigation into seismic responses of offshore structures, particularly subsea transportation tunnels, to ensure seismic stability. This study analyzes lining forces of deeply buried circular tunnels under P-waves on inclined seabeds, adopting a non-slip single-layer lining model. Section 1 establishes analytical methods for stress fields in permeable bedrock layers and corresponding lining force calculations. Section 2 examines how sedimentary layer parameters influence lining forces through case studies.

## 2 Computational Model

### 2.1 Model Introduction

This study investigates the seismic response of subsea tunnels in inclined seabed strata. The offshore site is modeled as a half-space comprising three layers: seawater, sedimentary layer, and bedrock, as illustrated in Figure 1. Adopting assumptions from Shan et al.<sup>[18]</sup>, seawater is idealized as a compressible inviscid fluid, the permeable bedrock is treated as a fluid-saturated poroelastic medium, and the bedrock layer is modeled as an isotropic homogeneous linear elastic material. Seismic waves propagate upward from the bedrock. The tunnel lining interface assumes stress and displacement continuity with a non-slip condition. The methodology involves first calculating the seismic-induced stress field at the tunnel location, followed by deriving internal forces in the lining based on the obtained stress distribution.

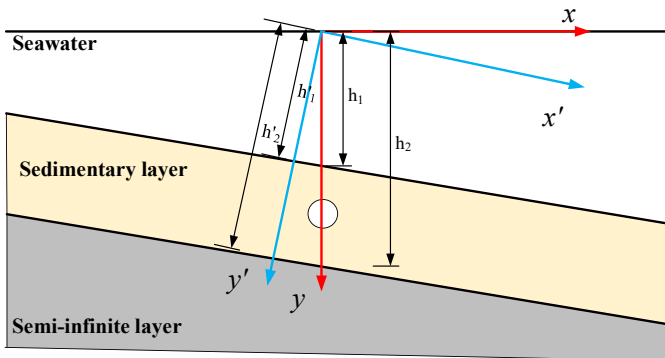


**Fig. 1.** Schematic diagram of the seawater-inclined seabed-bedrock system

Building on methodologies by EI Naggar et al.<sup>[1]</sup> and Zhao et al.<sup>[9]</sup>, which transform seismic wave interactions with tunnels in elastic half-spaces into equivalent loading

scenarios within an infinite elastic medium, this study calculates anisotropic stress components—hydrostatic and deviatoric —using effective stress at the tunnel centroid, as schematically shown in Figure 2.

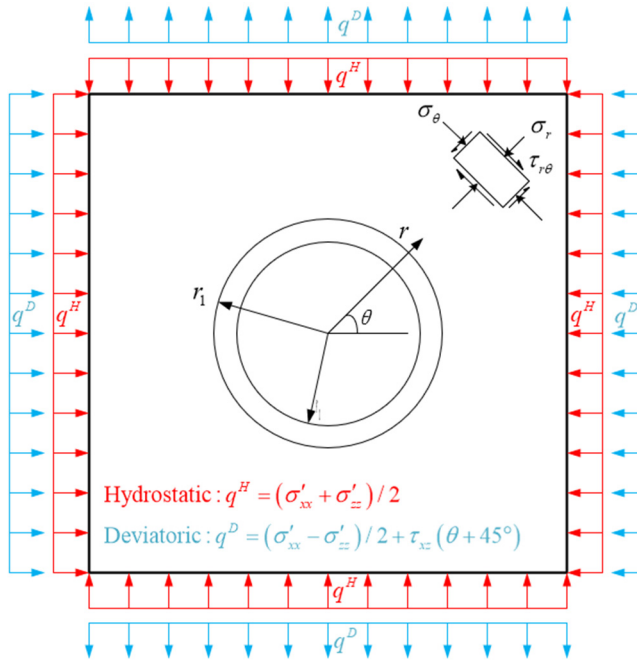


Fig. 2. Separation of the anisotropic loadings in ground induced by seismic waves

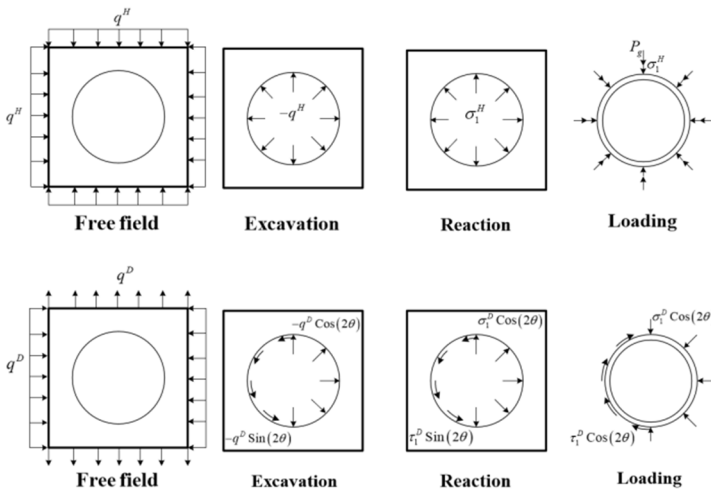


Fig. 3. Load decomposition without slippage

The tunnel's internal forces can be determined separately for these two components, with the final solution obtained through superposition. Following Zhao et al.<sup>[10]</sup>'s approach for non-slip lining interfaces, the hydrostatic and deviatoric stress components are calculated as:

$$\begin{aligned}
 q^H &= (\sigma'_{xx} + \sigma'_{zz}) / 2 \\
 q^D &= (\sigma'_{xx} - \sigma'_{zz}) / 2 + \tau_{xz} (\theta + 45^\circ) \\
 P_g &= p^F
 \end{aligned}
 \tag{1}$$

Under non-slip conditions, the loads acting on the seabed and tunnel are decomposed into the configurations illustrated in Figure 3.

### 2.2 Governing Equations and Solutions

The symbols used in the derivations throughout this section are defined in Table 1.

**Table 1.** Symbols of the basic equations

$\varphi^W$	Scalar displacement potential
$c_w$	Compressional wave speed
$\lambda$ & $\mu$	Lamé parameters of solid skeleton
$\mathbf{u}^S$ & $\mathbf{u}^F$	Solid and fluid displacement vectors, respectively
$\rho_s$ & $\rho_f$	Solid and pore-fluid particle density, respectively
$K_b$	Bulk modulus of the solid skeleton
$Q$	Biot's constants, $1/Q = (\alpha - n) / K_s + n / \lambda_f$
$\varphi^S$ & $\varphi^F$	Solid and fluid scalar displacement potentials, respectively
$\psi^S$ & $\psi^F$	Solid and fluid vector displacement potentials, respectively
$E_s$ & $E_L$	Young's modulus for the site and lining, respectively
$\mu_s$ & $\mu_L$	Poisson's ratio for the site and lining, respectively

For seawater idealized as an inviscid fluid, the displacement field is expressed as:

$$\nabla^2 \varphi^W = \frac{1}{c_w^2} \frac{\partial^2 \varphi^W}{\partial t^2}
 \tag{2}$$

The governing equations for solid-fluid displacements in saturated porous media (Simon et al.<sup>[19]</sup>; Biot et al.<sup>[20]</sup>) are formulated as:

$$\begin{aligned}
& \mu \nabla^2 \mathbf{u}^S + [\lambda + \mu + \alpha Q(\alpha - n)] \text{grad}(\text{div} \mathbf{u}^S) \\
& + \alpha Q n \text{grad}(\text{div} \mathbf{u}^F) = (1 - n) \rho_s \mathbf{u}_{,tt}^S + n \rho_F \mathbf{u}_{,tt}^F \\
& (\alpha - n) Q \text{grad}(\text{div} \mathbf{u}^S) + n Q \text{grad}(\text{div} \mathbf{u}^F) \\
& = \rho_F \mathbf{u}_{,tt}^F - b(\mathbf{u}_{,t}^S - \mathbf{u}_{,t}^F)
\end{aligned} \tag{3}$$

The solid and fluid displacement fields are expressed as:

$$\begin{aligned}
\mathbf{u}^S &= \nabla \varphi^S + \nabla \times \boldsymbol{\psi}^S, \nabla \cdot \boldsymbol{\psi}^S = 0 \\
\mathbf{u}^F &= \nabla \varphi^F + \nabla \times \boldsymbol{\psi}^F, \nabla \cdot \boldsymbol{\psi}^F = 0
\end{aligned} \tag{4}$$

For plane strain conditions, following Shan et al.'s framework (2023<sup>[18]</sup>, 2024a<sup>[21]</sup>, 2024b<sup>[22]</sup>), stress fields and pore pressure in saturated porous media are derived from displacement potentials through Equations (1)-(3). The stress field is formulated as:

$$\begin{aligned}
\sigma_{xx}^S &= (\lambda + 2\mu) \frac{\partial^2 \varphi^S}{\partial x^2} + \lambda \frac{\partial^2 \varphi^S}{\partial y^2} + 2\mu \frac{\partial^2 \psi^S}{\partial x \partial y} - \alpha p^F \\
\sigma_{yy}^S &= \lambda \frac{\partial^2 \varphi^S}{\partial x^2} + (\lambda + 2\mu) \frac{\partial^2 \varphi^S}{\partial y^2} - 2\mu \frac{\partial^2 \psi^S}{\partial x \partial y} - \alpha p^F \\
\sigma_{xy}^S &= \mu \left( 2 \frac{\partial^2 \varphi^S}{\partial x \partial y} + \frac{\partial^2 \psi^S}{\partial y^2} - \frac{\partial^2 \psi^S}{\partial x^2} \right) \\
-p^F &= (\alpha - n) Q \left( \frac{\partial^2 \varphi^S}{\partial x^2} + \frac{\partial^2 \varphi^S}{\partial y^2} \right) + n Q \left( \frac{\partial^2 \varphi^F}{\partial x^2} + \frac{\partial^2 \varphi^F}{\partial y^2} \right)
\end{aligned} \tag{5}$$

The non-slip condition at the ground-lining interface enforces continuity of tangential stresses. Under hydrostatic loading, radial displacements at the interface satisfy compatibility between the seabed and lining. Total radial displacement comprises three components: free-field displacement induced by hydrostatic stress, stress-relief displacement from tunnel excavation, and displacement caused by lining reaction forces. These are resolved via Hooke's law under plane strain conditions:

$$u_{r,L}^H = u_{r,g}^H = u_{r,g,free}^H + u_{r,g,exc}^H + u_{r,g,re}^H \tag{6}$$

Displacement under hydrostatic free-field loading:

$$u_{r,g,free}^H = \frac{(1 + \mu_g)(1 - 2\mu_g)r}{E_g} q^H \tag{7}$$

Hydrostatic excavation-induced displacement:

$$u_{r,g,exc}^H = \int \epsilon_{r,g,exc} dr = \frac{r_1^2 (1 + \mu_g)}{E_g r} q^H \tag{8}$$

Hydrostatic lining reaction-induced displacement:

$$u_{r,g,ve}^H = \int \epsilon_{r,g,ve} dr = -\frac{r_1^2(1 + \mu_g)}{E_g r} \sigma_1^H \tag{9}$$

Radial displacement from pore water pressure and radial reaction forces:

$$u_{r,L}^H = \frac{(1 + \mu_L)r}{E_L(1 - h_1)} \left[ \left( \frac{r_2^2}{r^2} + 1 - 2\mu_L \right) (P_g + \sigma_1^H) \right] \tag{10}$$

Substituting Eqs. (7)-(10) into Eq. (6) yields the radial stress at the seabed-lining interface under hydrostatic loading:

$$\sigma_1^H = \frac{2E_L(1 + \mu_g)(1 - \mu_g)(1 - h)q^H}{E_g(1 + \mu_L)(h + 1 - 2\mu_L) + E_L(1 + \mu_g)(1 - h)} - \frac{E_g(1 + \mu_L)(h + 1 - 2\mu_L)P_g}{E_g(1 + \mu_L)(h + 1 - 2\mu_L) + E_L(1 + \mu_g)(1 - h)} \tag{11}$$

Under deviatoric loading, kinematic compatibility requires equal radial and tangential displacements at the interface:

$$\begin{aligned} u_{r,g}^D = u_{r,L}^D &= u_{r,g,free}^H + u_{r,g,exc}^H + u_{r,g,ve}^H \\ u_{\theta,g}^D = u_{\theta,L}^D &= u_{\theta,g,free}^H + u_{\theta,g,exc}^H + u_{\theta,g,ve}^H \end{aligned} \tag{1}$$

The displacement components are:

$$\begin{aligned} u_{r,free}^D &= \frac{(1 + \mu_g)}{E_g} r q^D \cos(2\theta) \\ v_{\theta,free}^D &= -\frac{q^D \cdot (1 + \mu_g) \cdot r}{E_g} \sin(2\theta) \\ u_{r,g,exc}^D &= \frac{q^D \cdot (1 + \mu_g)}{E_g} \left[ 4 \cdot (1 - \mu_g) \cdot \frac{r_1^2}{r} - \frac{r_1^4}{r^3} \right] \cdot \cos(2\theta) \\ v_{\theta,g,exc}^D &= -\frac{q^D \cdot (1 + \mu_g)}{E_g} \left[ \frac{r_1^4}{r^3} + 2(1 - 2\mu_g) \frac{r_1^2}{r} \right] \sin(2\theta) \end{aligned} \tag{12}$$

$$\begin{aligned}
u_{r,g,ve}^D &= \frac{(1+\mu_g) \cdot r}{3 \cdot E_g} (-6 \cdot (1-\mu_g) \cdot (\sigma_1^D + \tau_1^D) \cdot \left(\frac{r_1}{r}\right)^2 \\
&\quad + (\sigma_1^D + 2\tau_1^D) \cdot \left(\frac{r_1}{r}\right)^4) \cdot \cos(2\theta) \\
v_{\theta,g,ve}^D &= \frac{(1+\mu_g) \cdot r}{3 \cdot E_g} ((\sigma_1^D + 2\tau_1^D) \cdot \left(\frac{r_1}{r}\right)^4 \\
&\quad - 3 \cdot (1-2 \cdot \mu_g) \cdot (\sigma_1^D + \tau_1^D) \cdot \left(\frac{r_1}{r}\right)^2) \sin(2\theta) \\
u_{r,L}^D &= \frac{2(1+\mu_L)r}{E_L} (-A_1 - 2\mu_L B_1 r^2 + \frac{C_1}{r^4} + 2(1-\mu_L) \frac{D_1}{r^2}) \\
v_{\theta,L}^D &= \frac{2(1+\mu_L)r}{E_L} (A_1 + (3-2\mu_L) B_1 r^2 + \frac{C_1}{r^4} - (1-2\mu_L) \frac{D_1}{r^2})
\end{aligned} \tag{13}$$

Substituting Equations (13)-(14) into Equation (12) yields the radial stress at the seabed-lining interface under deviatoric loading:

$$\begin{pmatrix} \sigma_1^D \\ \tau_1^D \end{pmatrix} = (C_L^{D3} C_L^{D1} - C_g^D)^{-1} \begin{pmatrix} \frac{(1+\mu_g)r_1 q^D}{E_g} (4-4\mu_j) \\ -\frac{(1+\mu_g)r_1 q^D}{E_g} (4-4\mu_j) \end{pmatrix} \tag{14}$$

By integrating stresses within the lining, thrust and bending moment are calculated using:

$$\begin{pmatrix} T_L \\ M_L \end{pmatrix} = C_L^{D4} C_L^{D1} \begin{pmatrix} \sigma_1^D \\ \tau_1^D \end{pmatrix} + \begin{pmatrix} r_1 (\sigma_1^H + P_j) \\ \frac{r_2^2}{1-h} \left[ \ln\left(\frac{r_1}{r_2}\right) + \frac{r_2^2 - r_1^2}{2r_1 r_2} \right] (\sigma_1^H + P_j) \end{pmatrix} \tag{15}$$

Where:

$$\begin{aligned}
 h &= (r_2 / r_1)^2 \\
 C_g^D &= \frac{(1 + \mu_g) r_1}{3E_g} \begin{pmatrix} 6\mu_g - 5 & 4 - 6\mu_g \\ 4 - 6\mu_g & 6\mu_g - 5 \end{pmatrix} \\
 C_L^{D1} &= \frac{1}{6(1-h)^3 r^2} \begin{pmatrix} -3(2h^2 + h + 1)r^2 & -6h^2 r^2 \\ 3h + 1 & 3h - 1 \\ -(h + 3)h^2 r^6 & -2h^3 r^6 \\ 3(h^2 + h + 2)hr^4 & 3(h^2 + h)hr^4 \end{pmatrix} \\
 C_L^{D3} &= \frac{2(1 + \mu_L) r}{E_L} \begin{pmatrix} -1 & -2\mu_L r^2 & r^{-4} & 2(1 - \mu_L) r^{-2} \\ 1 & (3 - 2\mu_L) r^2 & r^{-4} & -(1 - 2\mu_L) r^{-2} \end{pmatrix} \\
 C_L^{D4} &= \begin{pmatrix} 2(r_1 - r_2) \cos(2\theta) & 0 \\ 4(r_1^3 - r_2^3) \cos(2\theta) & (r_1^2 - r_2^2)(r_1 - r_2)^2 \\ -2(r_1^{-3} - r_2^{-3}) \cos(2\theta) & -2r_1^{-2} + 2r_2^{-2} - r_1 r_2^{-3} + r_1^{-3} r_2 \\ 0 & 0 \end{pmatrix}^T
 \end{aligned}$$

### 3 Case Study Analysis

#### 3.1 Model Parameters

The example in this paper makes the following assumptions: the input ground motion is a P-wave with acceleration amplitude 1 m/s<sup>2</sup> propagating upward from the bedrock; the depth of the seawater layer is 30m, the depth of the sediment layer is 60m, and the buried depth of the tunnel center point (calculated from the water-solid interface) is 30m; the outer radius and inner radius of the tunnel are set to 5.0m and 4.6m, respectively, and the Poisson's ratio and Young's modulus of the tunnel lining are set to 0.1 and 3.5×10<sup>5</sup>, respectively; see Table 2 for model parameters.

**Table 2.** Parameter table

Table 2. Parameter table	
Bulk modulus of seawater	2.0 GPa
Density of seawater	1000 Kg/m <sup>3</sup>
Density of soil	2650 Kg/m <sup>3</sup>
Lame's constants of soil	λ=18 MPa & μ=8.0 MPa
Porosity of soil	0.4
Permeability coefficient of soil	1×10 <sup>-3</sup> m/s
Damping ratio of soil	7%

Density of fluid	1000 Kg/m <sup>3</sup>
Bulk modulus of fluid	2.0 GPa
Density of Saturated sediment	2700 Kg/m <sup>3</sup>
Lame's constants of saturated sediment	$\lambda=1.5$ GPa & $\mu=1.0$ GPa
Porosity of saturated sediment	0.1
Permeability coefficient of saturated sediment	$5 \times 10^{-4}$ m/s
Damping ratio of saturated sediment	5%
Density of bedrock	2500 Kg/m <sup>3</sup>
Lame's constants of bedrock	$\lambda=6.5$ MPa & $\mu=4.5$ MPa

### 3.2 Model Validation

Under identical parameters, the stress calculation results of the proposed model at a 0° inclination angle were compared with those from Zhao et al.<sup>[10]</sup>'s horizontal seabed model, with the xx-direction stress comparison plot (Figure 4) serving as a representative example. As shown in Figure 4, the computed stress fields between the two models exhibit minimal discrepancies under horizontal seabed conditions, confirming the validity and reliability of the present study.

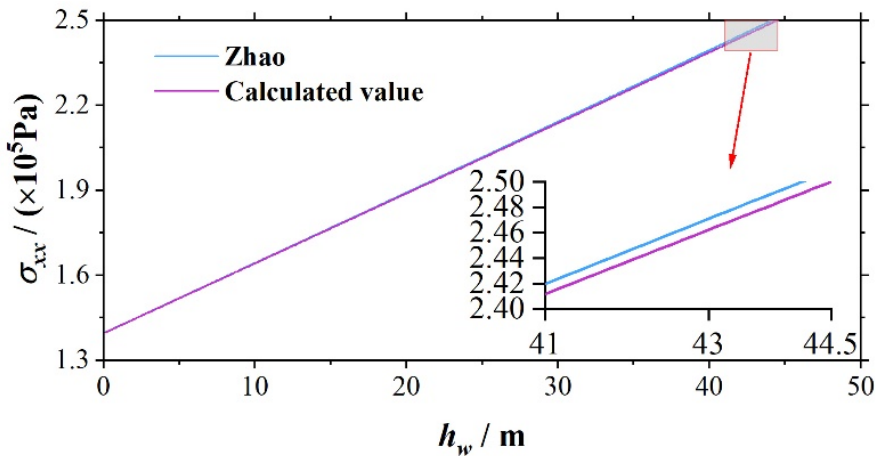


Fig. 4. xx-direction stress comparison plot

### 3.3 Parametric Analysis

**3.3.1 Seawater Layer Thickness.** By varying the seawater layer thickness from 20 m to 80 m, its influence on tunnel lining forces was analyzed. Selected lining force diagrams are shown in Figure 5.

Results indicate that the seabed inclination angle primarily affects the response to seismic motions below 0.1 Hz. As the seawater depth increases, the low-frequency amplitude of the tunnel response gradually amplifies overall, while high-frequency peaks emerge.

**3.3.2 Sedimentary Layer Thickness.** In the two-layer seabed configuration (comprising an upper soil layer and a lower permeable rock layer), this case study examines scenarios where the soil layer thickness ranges from 0 m to 10 m (upper stratum) and the permeable rock layer thickness adjusts correspondingly from 60 m to 50 m (lower stratum). Corresponding lining forces are illustrated in Figure 6.

Results demonstrate that in the seawater-sediment-bedrock model, maintaining the total sedimentary thickness while varying individual layer proportions significantly impacts lining forces. As the seabed inclination angle increases, the maximum lining force amplitudes exhibit distinct extrema at specific frequencies, with these extrema becoming more pronounced at steeper angles. Concurrently, increased soil layer thickness shifts the extremum frequencies toward lower ranges.

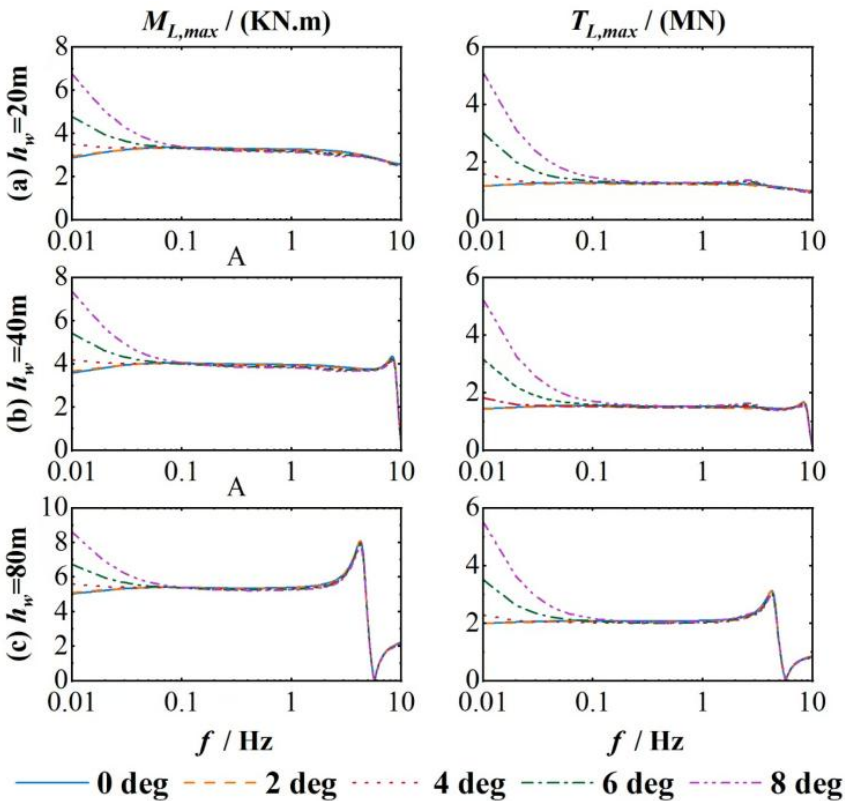


Fig. 5. The variation of moments and thrust with the depth of saturated sediment layer

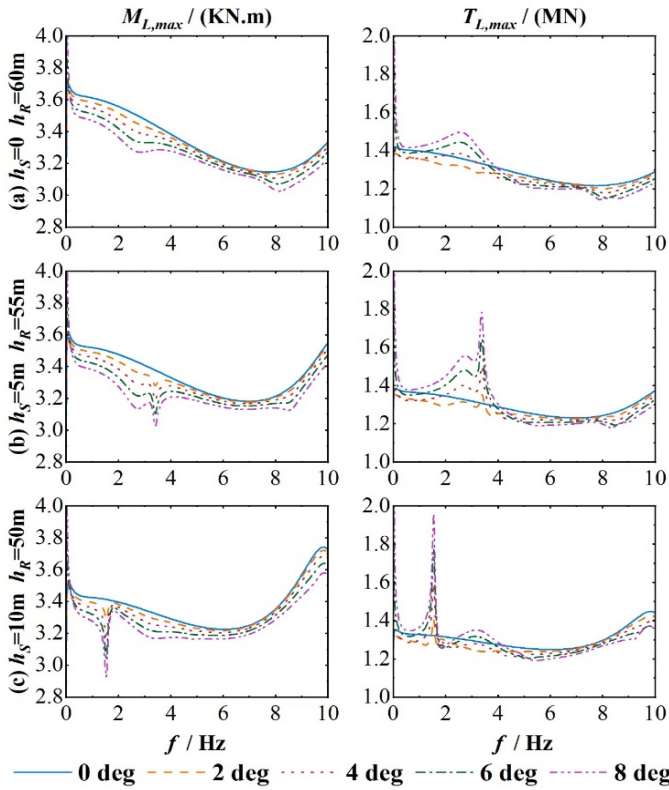


Fig. 6. The variation of moments and thrust with the depth of soil and rock

### 3.3.3 Permeability Coefficient

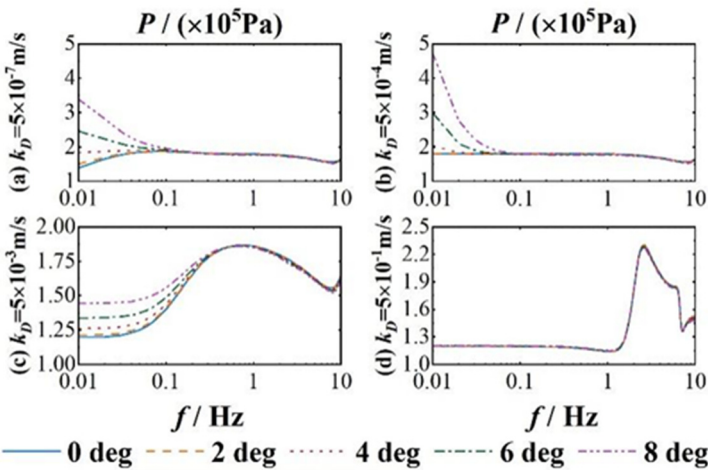


Fig. 7. The variation of stress field with frequency at different sloping angles

To investigate the influence of seabed sediment permeability on lining forces, parametric analyses were conducted with permeability coefficients ranging from  $5 \times 10^{-7}$  to  $5 \times 10^{-1}$ , focusing on the permeable rock layer. Stress field variations under different seabed inclination angles were first plotted against frequency. Given the wide permeability range, stress diagrams for characteristic permeability values with significant stress variations are shown in Figure 7.

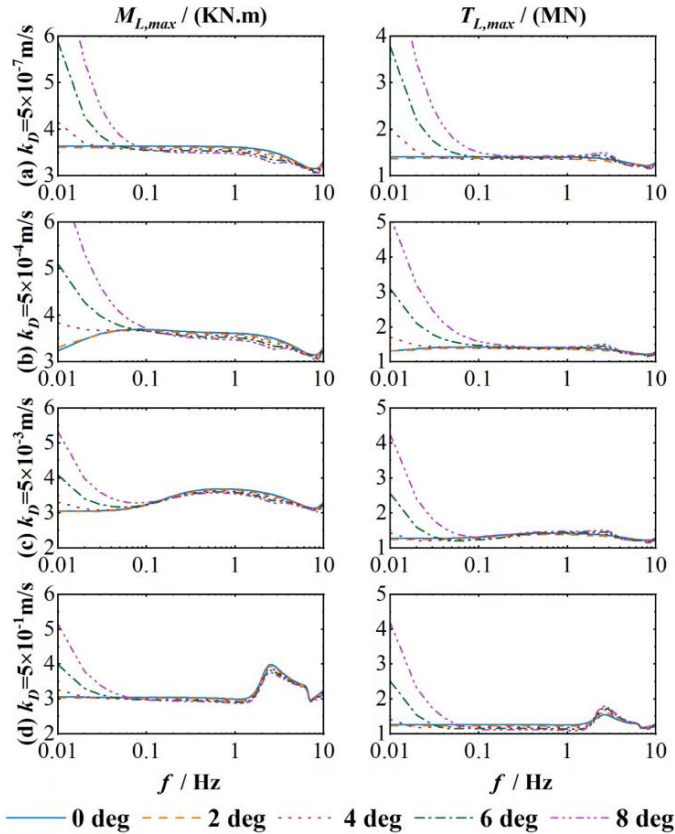


Fig. 8. The variation of stress field with frequency at different sloping angles

The results reveal that seabed inclination significantly affects pore water pressure under seismic motions below 0.1 Hz, with steeper angles amplifying low-frequency, long-period pore pressure amplitudes. However, increasing permeability weakens this inclination-dependent effect. Lining force variations under different permeability coefficients and inclination angles are illustrated in Figure 8.

Computational results demonstrate that seabed inclination primarily governs the maximum lining forces in low-frequency, long-period seismic motions ( $\leq 0.1$  Hz), with steeper angles exacerbating these effects. While increased permeability reduces inclination-induced pore pressure variations, the persistent influence of inclination on xx-

direction stress at low frequencies maintains notable differences in lining forces, albeit with diminished amplitude variations.

## 4 Conclusions

This study employs an offshore seabed model (seawater-sediment-bedrock) to compute stress fields at tunnel centers under P-wave excitation across varying seabed inclinations, deriving lining forces through cross-sectional analysis. Key findings from parametric studies on seawater layer thickness, sedimentary layer thickness and permeability include:

1. Seabed inclination drastically alters subsea tunnel seismic responses under long-period motions ( $>10$  s). Thrust and bending moments increase markedly with steeper angles.
2. Beyond the low-frequency range ( $<0.1$  Hz), inclination effects peak near the seabed's natural frequency, causing pronounced thrust/moment fluctuations.
3. Sediment permeability modulates inclination impacts: For fixed angles, reduced permeability elevates low-frequency lining forces due to amplified pore pressure coupling.

This study calculates the maximum internal forces of submarine tunnel linings under various parameters based on an inclined seabed model. Compared with numerical simulation methods, this approach proves simpler and more time-efficient, making it suitable for preliminary estimation of submarine tunnel linings in inclined seabeds while providing references for parameter selection in numerical simulations. However, the current study only focuses on the maximum internal forces of linings without calculating precise internal force distributions across lining cross-sections. Future research should consider analyzing internal force distributions while exploring the seismic response of structures when submarine sediment layers are composed of anisotropic materials. This investigation would better inform the design of offshore structures on submarine beds.

## References

1. HanyEl NaggarH. El Naggar, Sean D.HinchbergerS.D. Hinchberger, and K. Y.LoK.Y. Lo., A closed-form solution for composite tunnel linings in a homogeneous infinite isotropic elastic medium. *Canadian Geotechnical Journal*. 45(2): 266-287, 2008, doi:10.1139/T07-055.
2. Kontoe, S., Avgerinos, V., & Potts, D.M., Numerical validation of analytical solutions and their use for equivalent-linear seismic analysis of circular tunnels. *Soil Dynamics and Earthquake Engineering*, 66, 206-219, 2014.
3. Jingqi Huang, Huifang Li, Su Chen, Yawei Duan et.al., Simplified analytical solutions for seismic response on cross section of circular tunnel with composite linings, *Computers and Geotechnics*, Volume 136, 104169, ISSN 0266-352X, 2021, doi:10.1016/j.compgeo.2021.104169.

4. Duan Y , Zhao M , Huang J Q , Xiuli Du., Analytical Solution for Circular Tunnel under Obliquely Incident P Waves considering Different Contact Conditions[J].Shock and Vibration, 2021, doi:10.1155/2021/1946184.
5. Chen, G., Yu, H. & Bobet., A. Analytical Solution for Seismic Response of Deep Tunnels with Arbitrary Cross-Section Shape in Saturated Orthotropic Rock. *Rock Mech Rock Eng* 55, 5863–5878, 2022, doi:10.1007/s00603-022-02935-3
6. Mi Zhao, Yawei Duan, Jingqi Huang, Huifang Li et al., Analytical solutions for circular composite-lined tunnels under obliquely incident seismic SV and P waves, *Computers and Geotechnics*, Volume 151, 104939, ISSN 0266-352X, 2022, doi:10.1016/j.compgeo.2022.104939.
7. Yu, H., & Chen, G., Analytical solution for seismic response of deep tunnels covered by an isolation layer subjected to SH waves. *International Journal for Numerical and Analytical Methods in Geomechanics*, 1–15., 2022, doi:10.1002/nag.3623
8. Yawei Duan, Jingqi Huang, Xu Zhao, Mi Zhao et al., Analytical solutions for stresses and displacements of tunnels under static and seismic loading, *Computers and Geotechnics*, Volume 162, 105630, ISSN 0266-352X, 2023, doi:10.1016/j.compgeo.2023.105630.
9. Wusheng Zhao, Weizhong Chen, Diansen Yang, Hou Gao et al., Analytical solution for seismic response of tunnels with composite linings in elastic ground subjected to Rayleigh waves, *Soil Dynamics and Earthquake Engineering*, Volume 153, 107113, ISSN 0267-7261, 2022, doi:10.1016/j.soildyn.2021.107113.
10. Wusheng Zhao, Hou Gao, Weizhong Chen, Peiyao Xie., Analytical study on seismic response of subsea tunnels in a multi-layered seabed subjected to P- and SV-waves, *Tunnelling and Underground Space Technology*, Volume 134, 105015, ISSN 0886-7798, 2023, doi:10.1016/j.tust.2023.105015.
11. Feng AC, Price WG., Numerical simulations of the hydrodynamic responses of a body interacting with wave and current over a sloping seabed. *Appl Ocean Res.* 79:184-196, 2018.
12. Yuzhe Dou, Zhen Guo, Yangyang Gao, Lizhong Wang et al., Experimental investigations on the stability of clayey sloping seabed under wave actions, *Ocean Engineering*, Volume 239, 109805, ISSN 0029-8018, 2021, doi:10.1016/j.oceaneng.2021.109805.
13. Pu Xu, Zhixin Du, Ting Zhang, Baochun Chen., Vector form intrinsic finite element analysis of deepwater J-laying pipelines on sloping seabed, *Ocean Engineering*, Volume 247, 110709, ISSN 0029-8018, 2022, doi:10.1016/j.oceaneng.2022.110709.
14. Seyfipour, A. Walker., Thermo-mechanical walking of straight and continuous-snake-laid pipelines on sloping seabeds, *Applied Ocean Research*, Volume 94, 101980, ISSN 0141-1187, 2020, doi:10.1016/j.apor.2019.101980.
15. Amin Rafiei, M.S. Rahman, M.A. Gabr., Coupled analysis for response and instability of sloping seabed under wave action, *Applied Ocean Research*, Volume 88, Pages 99-110, ISSN 0141-1187, 2019, doi:10.1016/j.apor.2019.04.017.
16. H.-Y. Zhao, D.-S. Jeng., Numerical study of wave-induced soil response in a sloping seabed in the vicinity of a breakwater, *Applied Ocean Research*, Volume 51, Pages 204-221, ISSN 0141-1187, 2015, doi:10.1016/j.apor.2015.04.008.
17. Yun-Lin Ni, Bin Teng., Bragg resonant reflection of water waves by a Bragg breakwater with porous rectangular bars on a sloping permeable seabed, *Ocean Engineering*, Volume 235, 109333, ISSN 0029-8018, 2021, doi:10.1016/j.oceaneng.2021.109333.
18. Shan, Z., Xie, Z., Dong et al., An analytical solution for the dynamic response of a seawater-sloping seabed-bedrock system under an oblique incident P wave. *Int. J. Numer. Anal. Methods Geomech.* 47, 2136-2152, 2023, doi:10.1002/nag.3555.

19. Simon, B. R., Zienkiewicz, O. C., & Paul, D. K., An analytical solution for the transient response of saturated porous elastic solids. *International Journal for Numerical and Analytical Methods in Geomechanics*, 8, 381–398, 1984.
20. Biot, M. A., Theory of propagation of elastic waves in a fluid-saturated porous solid. I. Low-frequency range. *The Journal of the Acoustical Society of America*, 28(2), 168–178, 1956.
21. Shan, Z., Xie, Z., Li et al., An analytical solution for the dynamic response of a seawater-sloping seabed-bedrock system under an oblique incident SV wave. *Int. J. Numer. Anal. Methods Geomech.* 48, 463-475, 2024a, doi:10.1002/nag.3646.
22. Shan, Z., Xie, Z., Li et al., Analytical solution for the seismic response of a nearly saturated sloping seabed: Weak interlayer. *Ocean Eng.* 300, 117191, 2024b, doi:10.1016/j.oceaneng.2024.117191.

**Open Access** This chapter is licensed under the terms of the Creative Commons Attribution-NonCommercial 4.0 International License (<http://creativecommons.org/licenses/by-nc/4.0/>), which permits any noncommercial use, sharing, adaptation, distribution and reproduction in any medium or format, as long as you give appropriate credit to the original author(s) and the source, provide a link to the Creative Commons license and indicate if changes were made.

The images or other third party material in this chapter are included in the chapter's Creative Commons license, unless indicated otherwise in a credit line to the material. If material is not included in the chapter's Creative Commons license and your intended use is not permitted by statutory regulation or exceeds the permitted use, you will need to obtain permission directly from the copyright holder.

